Neuroelectric source localization by random spatial sampling

F. Pitolli [*], C. Pocci [†]

Dip. SBAI, Università di Roma "La Sapienza"
Via A. Scarpa 16, 00161 Roma, Italy

(2016)

Abstract

The magnetoencephalography (MEG) aims at reconstructing the unknown neuroelectric activity in the brain from the measurements of the neuromagnetic field in the outer space. The localization of neuroelectric sources from MEG data results in an ill-posed and ill-conditioned inverse problem that requires regularization techniques to be solved. In this paper we propose a new inversion method based on random spatial sampling that is suitable to localize focal neuroelectric sources. The method is fast, efficient and requires little memory storage. Moreover, the numerical tests show that the random sampling method has a high spatial resolution even in the case of deep source localization from noisy magnetic data.

Keywords:Neuroimaging; Magnetoencephalography; Inverse Problem; Random Sampling
MSC 2010]: 92C55, 47A52, 65R32

1 Introduction

Magnetoencephalography (MEG) ([13]) is a completely non-invasive imaging technique to map the neuroelectric activity from the measurements of

[*]francesca.pitolli@sbai.uniroma1.it
[†]cristina.pocci@sbai.uniroma1.it

the magnetic field that the activity itself induces outside the head. Due to its high temporal resolution - in the millisecond scale ([3]) - MEG is particularly attractive for mapping fast cerebral responses to spontaneous and/or evoked stimuli. From the analysis of the temporal evolution of the measured magnetic field distribution we can infer just partial information on the localization of active brain regions. In order to better focus neuroelectric sources, we have to solve the neuroelectric inverse problem aiming at reconstructing the neuronal current image once a measured magnetic field distribution outside the head is given.

Since the magnetic field decreases very fast as the distance between the electric sources and the sensor sites increases, the measured magnetic field may be very weak. For this reason MEG magnetometers are equipped with SQUIDs (Superconducting Quantum Interference Devices), which are very sensitive detectors of the magnetic flux ([13]). Moreover, MEG measurements are affected by high noise due to electromagnetic sources in the external environment and to the bioelectric activity generated by the muscular activity of the patient himself. Usually, these disturbances generate a magnetic signal of strength comparable with the signal of interest.

Another challenge of MEG is in its ill-conditioned nature; in fact, the radial - w.r.t. the inner skull - component of the neuroelectric current does not produce any magnetic field in the outer space and cannot be detected. This means that a single measured field could be generated by an infinite number of current distributions and further assumptions could be made in order to force the inverse problem to have a unique solution ([11]).

When solving the MEG inverse problem, we are interested in reconstructing the neuroelectric current image with high accuracy - in the order of few millimeters - having available only few magnetic data - usually, a few hundreds. Thus, the MEG inverse problem can be seen as an inverse problem with incomplete data. On the other hand, neurophysiologic studies have put in evidence that the neuroelectric current distribution is localized in small regions of the brain, i.e. the neuroelectric current distribution is spatially sparse. As a consequence, it is reasonable to expect that only few elementary sources might be sufficient to characterize and reconstruct the unknown current vector ([2, 4, 6]).

After these observations, in this paper we propose a new method based on random sampling, suitable to solve the MEG inverse problem under the sparsity assumption. The key ingredient of the method lies in the fact that we represent the electric current distribution we want to reconstruct by a

sample ensemble of few *localized* elementary sources. Under the sparsity assumption, just few elementary sources, randomly chosen from a large dictionary, are sufficient to well reconstruct the unknown current distribution. Some first results on the solution of the MEG inverse problem by the random sampling method can be found in ([1]) where it is shown that random sampling reduces significantly the ill-conditioning of the inverse problem so acting as a regularization technique. Moreover, the algorithm requires little memory storage and is very fast. Here, we deal with the problem of localizing focal deep sources from noisy magnetic data and show that the random sampling method combined with a shrinkage method has a high spatial resolution so that it can be effectively used in neuroimaging applications.

The paper is organized as follows. In Section 2, we recall the model usually used to describe the MEG forward problem and set the MEG inverse problem. In Section 3 we describe the random sampling method for the solution of the MEG inverse problem. Section 4 is devoted to several numerical tests showing the good performances of the proposed method. Finally, Section 5 contains some comments and conclusions.

2 The MEG forward and inverse problems

Following the classical model by Geselowitz ([7, 8]), we describe the head as a conductor consisting of homogeneous, nested, non intersecting regions, V_i, $i = 0, \dots m$, each one having constant conductivity, σ_i. In the following we assume that the neuroelectric current flows just inside the innermost region V_0, which represents the brain. From the quasi-static Maxwell's equations, it follows that the electric current density $\mathbf{J}(\mathbf{r})$ flowing in V_0, and the external magnetic field $\mathbf{B}(\mathbf{r})$, with $\mathbf{r}$ outside V_m, are related by the *Biot-Savart law*

$$\mathbf{B}(\mathbf{r}) = \frac{\mu_0}{4\pi} \int_{V_0} \frac{\mathbf{J}(\mathbf{r}') \times (\mathbf{r} - \mathbf{r}')}{|\mathbf{r} - \mathbf{r}'|^3} \, d\mathbf{r}' \,, \tag{2.1}$$

where μ_0 is the magnetic permeability in the vacuum.
The magnetometers are located in N sites, $\mathbf{q}_i, i = 1, \dots, N$, that belong to a surface Σ external to the head. Each magnetometer measures the magnetic field along the direction $\mathbf{e}(\mathbf{q}_i)$, which is the normal w.r.t. Σ in $\mathbf{q}_i$. Now, let $\mathcal{B}_{\mathbf{e}}(\mathbf{q}_i, \mathbf{J}) := \mathbf{B}(\mathbf{q}_i) \cdot \mathbf{e}(\mathbf{q}_i)$ be the integral operator relating the neuroelectric current and the magnetic field it generates in $\mathbf{q}_i$, projected along $\mathbf{e}(\mathbf{q}_i)$. Recalling that for any three vectors in $\mathbb{R}^3$ it holds $(\mathbf{v} \times \mathbf{w}) \cdot \mathbf{z} = -(\mathbf{z} \times \mathbf{w}) \cdot \mathbf{v}$,

we obtain the relation

$$\mathcal{B}_{\mathbf{e}}(\mathbf{q}_i, \mathbf{J}) = \frac{\mu_0}{4\pi} \int_{V_0} \left(\mathbf{e}(\mathbf{q}_i) \times \frac{\mathbf{r}' - \mathbf{q}_i}{|\mathbf{r}' - \mathbf{q}_i|^3} \right) \cdot \mathbf{J}(\mathbf{r}\,')\, d\mathbf{r}\,', \tag{2.2}$$

which is linear w.r.t. $\mathbf{J}$ (here, $\mathbf{v} \times \mathbf{w}$ and $\mathbf{v} \cdot \mathbf{w}$ are the usual cross and scalar products of vectors in $\mathbb{R}^3$, respectively, and $|\mathbf{v}|$ is the Euclidean norm).

In a realistic head geometry the forward MEG problem cannot be solved analytically, therefore numerical methods are needed. Usually, to solve numerically the forward problem, Boundary Element Method, Finite Element Method or Finite Difference Method are used ([9, 14]). All these methods require a large number of computational points to achieve high spatial resolution so that they both require high memory storage and have high computational load.

Having at hand the forward model, we can set the MEG inverse problem. This consists in estimating the neuroelectric current distribution $\mathbf{J}$ from the measurements of the external magnetic field, $G_i, i = 1, \ldots, N$. Therefore, the MEG inverse problem lies in minimizing the discrepancy

$$\Delta(\mathbf{J}) = \sum_{i=1}^{N} (G_i - \mathcal{B}_{\mathbf{e}}(\mathbf{q}_i, \mathbf{J}))^2\,, \tag{2.3}$$

w.r.t. the current distribution $\mathbf{J}$, once the measurements $G_i, i = 1, \ldots, N$, are given. Since the integral operator (2.2) has a non-trivial kernel, additional constraints, coming from the physics of the problem, have to be added so that the inverse problem has a unique solution ([5, 11]). This a priori information must be included into the inversion method to produce a physically meaningful solution. Our aim is to use sparsity assumption and random sampling to reduce the dimensionality of the inverse problem and, at the same time, its ill-conditioning.

3 The random sampling method

To solve the inverse problem we model the total current as a sum of a finite number of *elementary sources*, i.e.

$$\mathbf{J}(\mathbf{r}) \approx \sum_{k=1}^{M} \mathbf{J}_k\, \psi_k(\mathbf{r}\,)\,, \tag{3.1}$$

where $\mathbf{J}_k = (J_k^x, J_k^y, J_k^z)$ is the current intensity of the k elementary source having spatial distribution ψ_k.

Dealing with the localization of focal neural sources, it makes sense to assume the k elementary source to be a point-like source located in $\mathbf{r}_k \in V_0$, i.e. $\psi_k(\mathbf{r}) = \delta(\mathbf{r}_k - \mathbf{r})$, so that

$$\mathbf{J}(\mathbf{r}) \approx \sum_{k=1}^{M} \mathbf{J}_k \, \delta(\mathbf{r}_k - \mathbf{r}) \,, \tag{3.2}$$

where δ is the Dirac delta function.
Substituting (3.2) in (2.2), we obtain the discretized version of the forward operator $\mathcal{B}_{\mathbf{e}}(\mathbf{q}_i, \mathbf{J})$, i.e.

$$\mathcal{B}_{\mathbf{e}}(\mathbf{q}_i, \mathbf{J}) \approx \frac{\mu_0}{4\pi} \frac{1}{M} \sum_{k=1}^{M} \left(\mathbf{e}(\mathbf{q}_i) \times \frac{\mathbf{r}_k - \mathbf{q}_i}{|\mathbf{r}_k - \mathbf{q}_i|^3} \right) \cdot \mathbf{J}_k \,, \tag{3.3}$$

from which we obtain the so called lead-field matrix B with entries given by

$$B_{ik}^l = \frac{\mu_0}{4\pi} \frac{1}{M} \left(\mathbf{e}(\mathbf{q}_i) \times \frac{\mathbf{r}_k - \mathbf{q}_i}{|\mathbf{r}_k - \mathbf{q}_i|^3} \right)_l \,, \tag{3.4}$$

for $i = 1, \ldots, N$, $k = 1, \ldots, M$, $l = x, y, z$.

The MEG inverse problem consists in determining a configuration of the current density vector $J = [\mathbf{J}_1, \ldots, \mathbf{J}_M]^T$ that minimizes the discrepancy $\Delta(J) := \|BJ - G\|^2_{\mathbb{R}^N}$ once the set of the magnetic measurements $G = [g_1, \ldots, g_N]^T$ is given.

Since the current density we want to reconstruct can be assumed to be spatially sparse, i.e. non negligible just in few small regions of the brain, just few elementary sources with a *small* support are sufficient to reconstruct with a high accuracy the neuroelectric current distribution ([2, 4, 6]). In the random sampling method the elementary sources are randomly extracted from a large dictionary. To this end we select a sample ensemble of few random computational points, $\mathcal{R} = \{\mathbf{r}_k \in V_0, k = 1, \ldots M\}$, uniformly distributed inside V_0. The number of random points M can be chosen in the order of the number of measurements N so reducing the ill-conditioning of the matrix B and making the minimization of the discrepancy feasible. This is equivalent to select randomly few elementary sources $\psi_k(\mathbf{r})$.
The accuracy of the localization can be increased by performing a few runs,

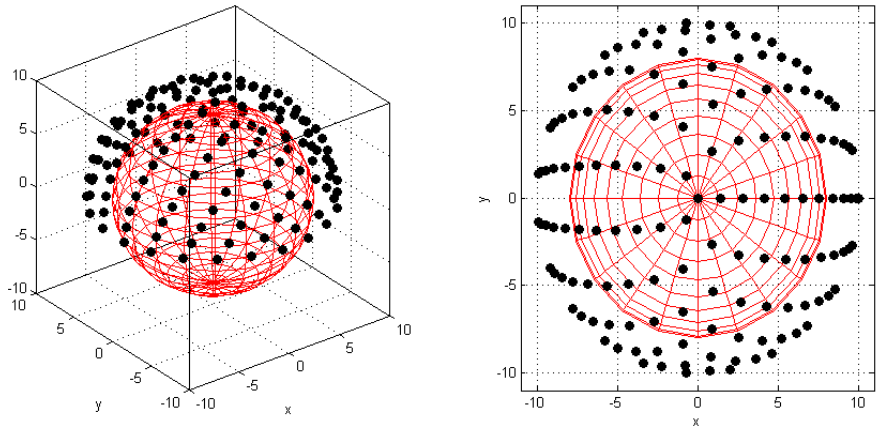

Figure 1: The conducting sphere (red grid) and the magnetometer sites (black circles).

each one with a different sample $\mathcal{R}$. In this case the source localization will be the mean of all the localizations obtained in each run. As the examples in the next section show, the random sampling method allows us to well localize superficial sources while it fails when the sources are deep. In this latter case a regularization term based on l_1-norm has to be added ([10]).

4 Numerical tests

To test the performances of the random sampling method we ran several tests on synthetic data. The data were generated by one or more current dipole sources located inside a spherical homogeneous conducting volume. The synthetic magnetic data were generated by sampling the radial component of the magnetic field in $N = 144$ sites distributed on a hemispherical surface concentric to the conducting sphere. In the tests the conducting sphere had radius $R = 8\,cm$ while the magnetometer sites were located on an hemisphere of radius $R_{mag} = 10\,cm$ (see Fig. 1)[1].

The different ensembles of computational points were extracted from a uniform grid filling the whole sphere having step size $h = 0.4\,cm$, so that the uniform grid had about 30000 points. We performed different runs extracting

[1]All the figures are in colors in the electronic version of the paper

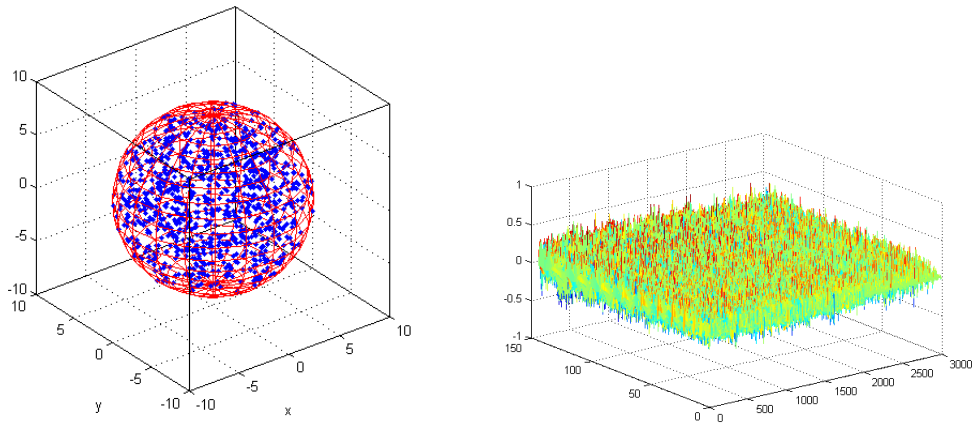

Figure 2: Left: A sample ensamble of $M = 1000$ computational random points uniformly distributed in the conducting sphere. Right: The amplitude of the entries of the discretization matrix B corresponding to the ensemble shown on the left.

in each one a different number of random points, ranging from $M = 500$ up to $M = 8000$, uniformly distributed inside the sphere. As an example, the point distribution for a sample ensemble of $M = 1000$ computational points is shown in Fig. 2 (left) while the corresponding discretization matrix B is shown in Fig. 2 (right). Note that to better localize deep sources we used a standard preconditioning technique based on the column balancing of the matrix B.

We tested the method on two sets of synthetic data. The first set was generated by a single current dipole, located at two different depths below the surface of the conducting sphere (Section 4.1). The second set was generated by three extended sources inside the conducting sphere (Section 4.2). The runs were performed on a laptop and took just a few seconds for each trial.

4.1 A single source in a homogeneous conducting sphere

In the first test the electric source was superficial, with depth $S_d = 1\,cm$ below the surface of the conducting sphere. The synthetic data are shown in Fig 3.

To solve the inverse problem we used different numbers of computational

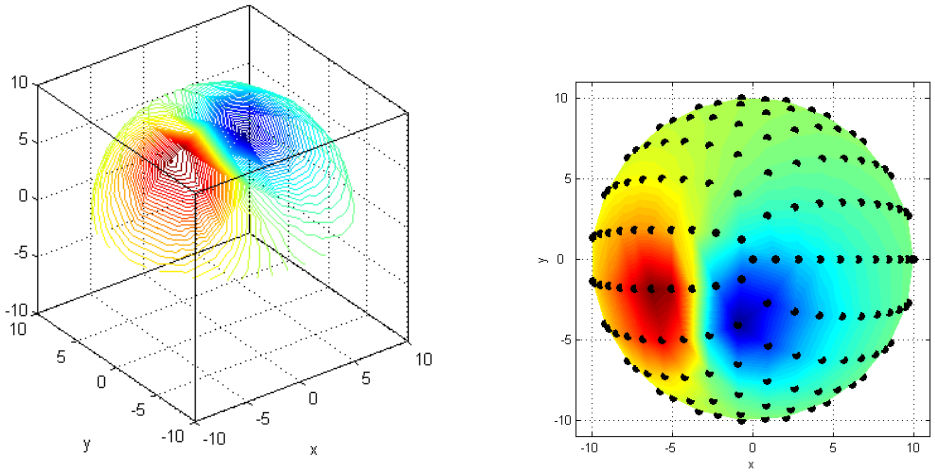

Figure 3: The magnetic data generated by a single source at depth $S_d = 1\,cm$.

points M and different numbers of trials N_t. As M and N_t increase, the reconstructed current density becomes more and more accurate. This is put in evidence in Figs. 4-5 where the reconstructed current intensity is shown for $M = 500$, $N_t = 10$ - a total of 5000 points - and $M = 4000$, $N_t = 20$ - a total of 80000 points - respectively. Note that since the computational points were chosen independently from a trial to another, different samples may contain some identical points.

In the second test the electric source was deeper with $S_d = 3\,cm$. The reconstructed current intensity is shown in Figs. 6-7 for $M = 500$, $N_t = 10$ and $M = 4000$, $N_t = 20$, respectively.

To better understand how the values of M and N_t affect the accuracy of the localization, we evaluated the localization distance error (LDE_{max}), defined as the distance between the point where the current dipole generating the data is located, and the point where the reconstructed electric current intensity has its maximum. A more significant error measure is the distance between the source position and the mean of the points in the region of interest (ROI), i.e. the region where the current intensity is highest (LDE_{mean}). Fig. 8 shows the behavior of LDE_{max} and LDE_{mean} as a function of the number of computational points. We used $M = 500, 1000, 2000, 4000, 8000$, computational points and performed $N_t = 5, 10, 20, 30, 40, 50$, trials with a different sample ensemble for each value of N_t. To be sure that LDE did not depend significantly on the ensemble $\mathcal{R}$ we used at each trial, for each value of M and

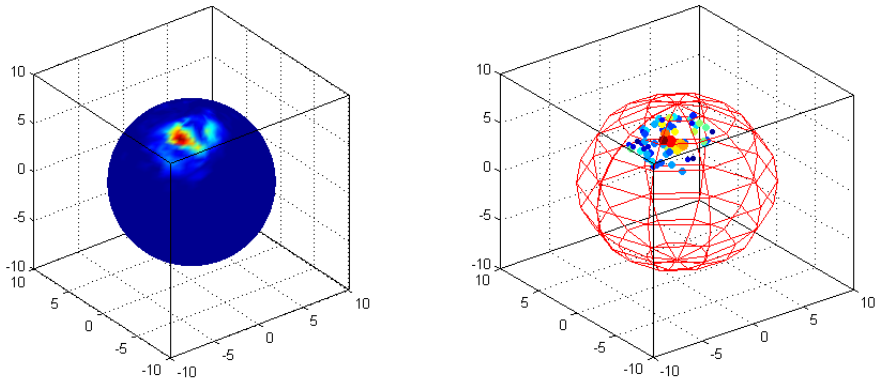

Figure 4: The reconstructed electric current intensity for $M = 500$ and $N_t = 10$ when $S_d = 1\,cm$. Left: The electric intensity on the surface of the conducting sphere. Right: The electric intensity in the computational points. Just the points where the intensity is significant are shown.

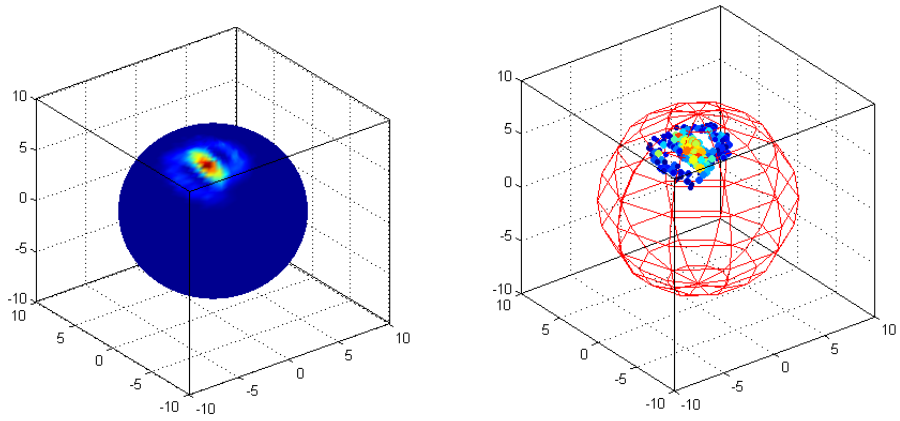

Figure 5: The reconstructed electric current intensity for $M = 4000$ and $N_t = 20$ when $S_d = 1\,cm$. Left: The electric intensity on the surface of the conducting sphere. Right: The electric intensity in the computational points. Just the points where the intensity is significant are shown.

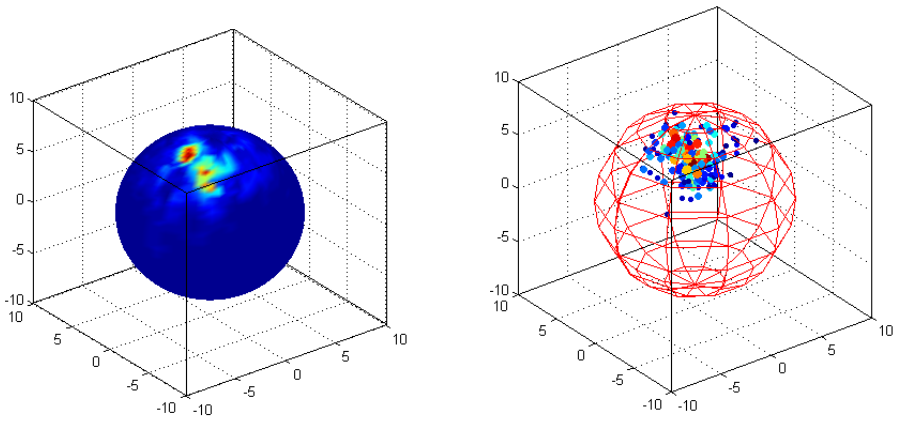

Figure 6: The reconstructed electric current intensity for $M = 500$ and $N_t = 10$ when $S_d = 3\,cm$. Left: The electric intensity on the surface of the conducting sphere. Right: The electric intensity in the computational points. Just the points where the electric intensity is significant are shown.

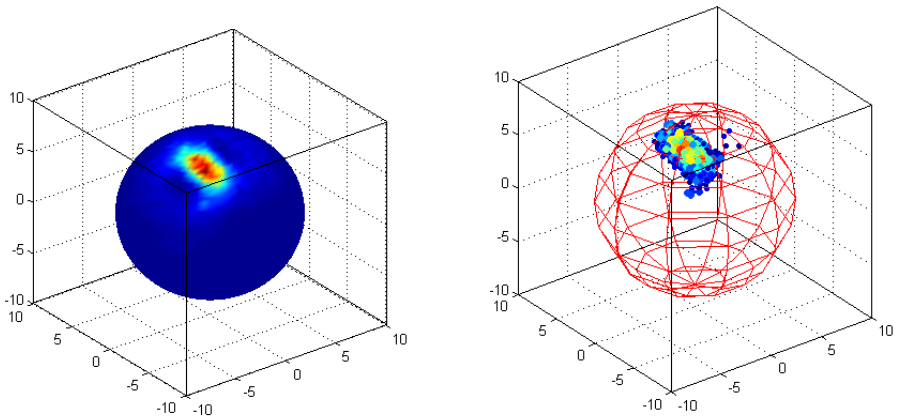

Figure 7: The reconstructed electric current intensity for $M = 4000$ and $N_t = 20$ when $S_d = 3\,cm$. Left: The electric intensity on the surface of the conducting sphere. Right: The electric intensity in the computational points. Just the points where the electric intensity is significant are shown.

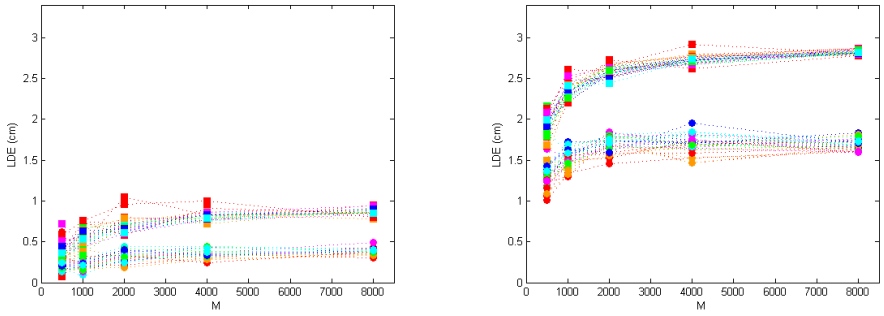

Figure 8: LDE_{max} (higher lines) and LDE_{mean} (lower lines) as a function of the number of computational points for $S_d = 1\,cm$ (left) and $S_d = 3\,cm$ (right). For each value of M the number of trials N_t varies from 5 to 50 ($N_t = 5$ (red), 10 (orange), 20 (violet), 30 (green), 40 (blue), 50 (cyan)).

N_t we solved the problem 5 times, each time using different ensembles of computational points. This gave rise to a little spread of the LDE. The graphs show that even if the spread decreases as the number of points increases, LDE slightly increases as M increases. Actually, when using all the points of the uniform grid we obtain $LDE_{max} = 1.1\,cm$ and $LDE_{mean} = 0.8\,cm$ for $S_d = 1\,cm$ and $LDE_{max} = 2.9\,cm$, and $LDE_{mean} = 1.9\,cm$ for $S_d = 3\,cm$. These values are very close to the values obtained for $M = 8000$.
We observe that the best results are obtained when running 30 trials with 500 points for each trial - less than the 0.2 % of all the points of the uniform grid - resulting in a total of 15000 points, possibly overlapping.

In the previous tests we solved the inverse problem by the least square method. Even if the method gives a rather small localization error in the case of the superficial source, the accuracy in the localization of the deep source is poor. In order to improve the localization of deep sources we used a shrinkage method based on ℓ_1-penalization as a regularization term ([10]).

In Fig. 9 the localization error as a function of M and N_t when using a shrinkage method is shown. In this case LDE_{max} and LDE_{mean} have approximately the same values and they do not much depend on the number of points. In particular, the error is in the order of $0.3\,cm$ as soon as $N_t \geq 20$, even in case of depth $S_d = 3\,cm$.

The shrinkage method can be used also to improve the localization when the data are affected by noise. In Figs. 10-11 the reconstructed current

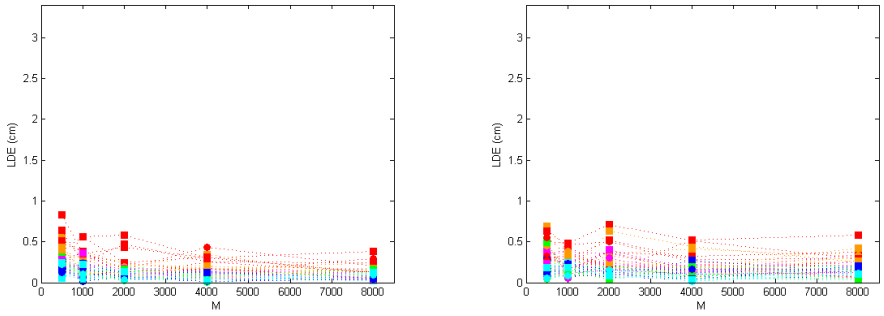

Figure 9: LDE_{max} and LDE_{mean} as a function of the number of computational points for $S_d = 1\,cm$ (left) and $S_d = 3\,cm$ (right) when the shrinkage method was used. For each value of M the number of trials N_t varies from 5 to 50 ($N_t = 5$ (red), 10 (orange), 20 (violet), 30 (green), 40 (blue), 50 (cyan)).

intensity when the magnetic data were corrupted by a Gaussian noise with s.n.r. $= 5$ is shown. The localization error is in the order of $2\,cm$ when using least square method while reduces to less than $1\,mm$ when using the shrinkage method.

4.2 Extended sources in a homogeneous conducting sphere

A more realistic example is the case when the magnetic data are generated by more extended sources. We simulated a single extended source as a set of several current dipoles confined in a small ball of radius $0.5\,cm$, located inside the conducting sphere. The synthetic data for three extended sources at depth $S_d = 1\,cm$ and $S_d = 3\,cm$ are shown in Fig. 12 and Fig. 13, respectively.

The reconstructed current intensity is shown in Figs. 14-15. The method correctly identifies the three sources but the localization suffers from a shift towards the surface of the conducting sphere. This effect is higher for weak sources, that is the source below right in Fig. 14 and all the three sources in Fig. 15. On the other hand shrinkage methods favor density current configurations where just the strongest sources are well detected (see Figs. 16-17).

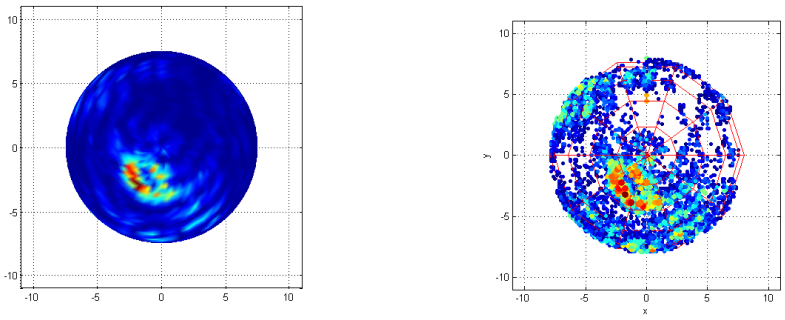

Figure 10: The reconstructed electric current intensity for $M = 4000$ and $N_t = 20$ for noisy data. Here, $S_d = 1\,cm$. Left: The electric intensity on the surface of the conducting sphere. Right: The electric intensity in the computational points. Just the points where the intensity is significant are shown.

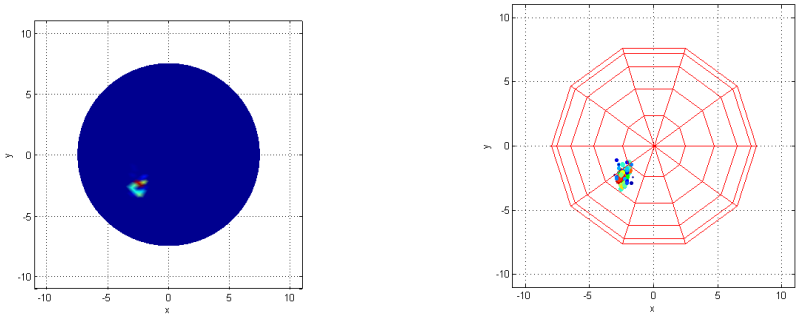

Figure 11: The reconstructed electric current intensity for $M = 4000$ and $N_t = 20$ for noisy data when the shrinkage method was used. Here, $S_d = 1\,cm$. Left: The electric intensity on the surface of the conducting sphere. Right: The electric intensity in the computational points. Just the points where the intensity is significant are shown.

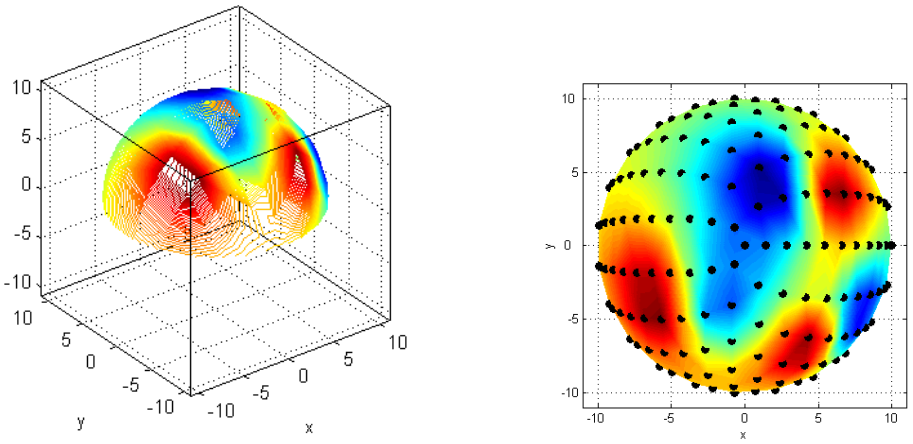

Figure 12: The magnetic data generated by three extended sources at depth $S_d = 1\,cm$.

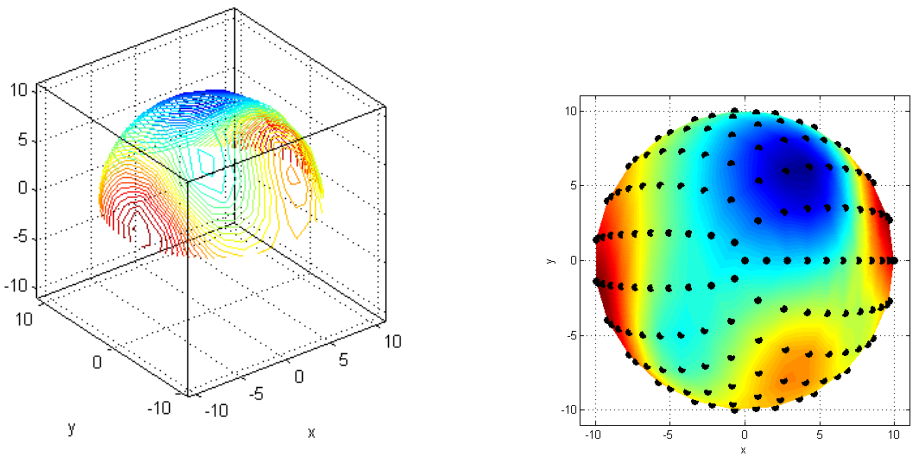

Figure 13: The magnetic data generated by three extended sources at depth $S_d = 3\,cm$.

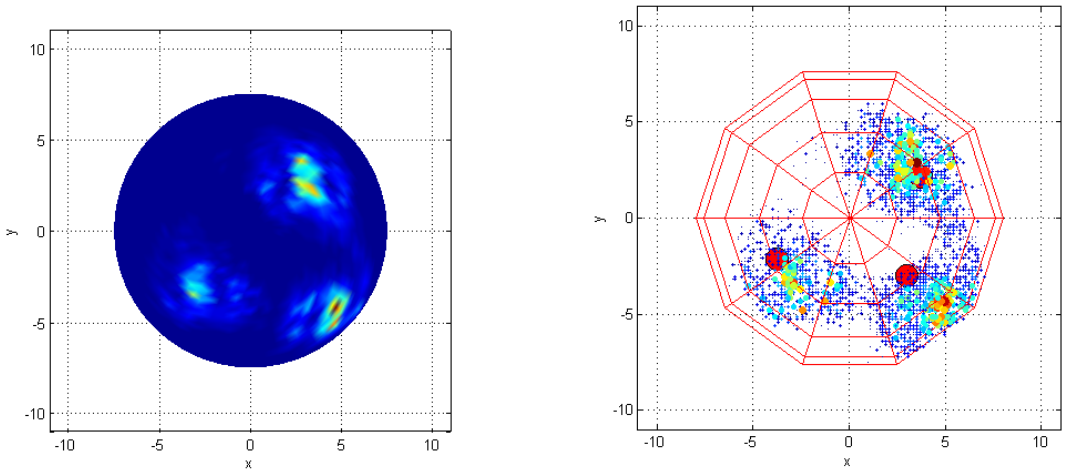

Figure 14: The reconstructed electric current intensity for three extended sources (red circles) at depth $S_d = 1\,cm$. Here, $M = 2000$ and $N_t = 20$. Left: The electric intensity on the surface of the conducting sphere. Right: The electric intensity in the computational points. Just the points where the intensity is significant are shown.

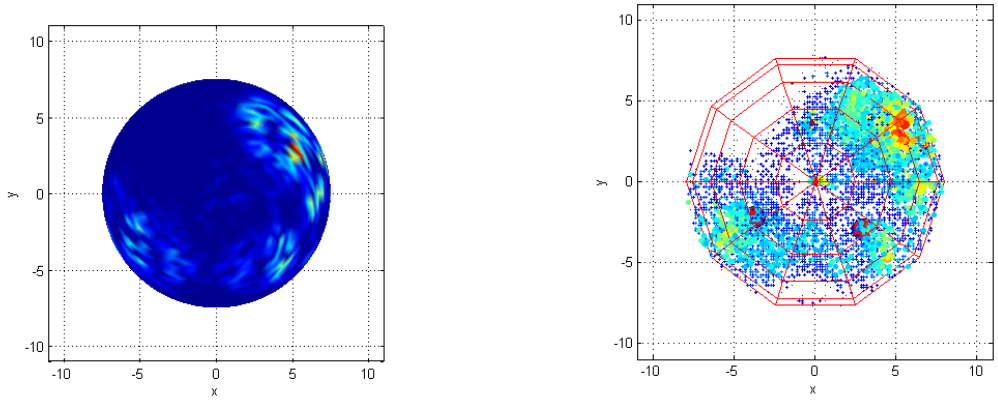

Figure 15: The reconstructed electric current intensity for three extended sources (red circles) at depth $S_d = 3\,cm$. Here, $M = 2000$ and $N_t = 20$. Left: The electric intensity on the surface of the conducting sphere. Right: The electric intensity in the computational points. Just the points where the intensity is significant are shown.

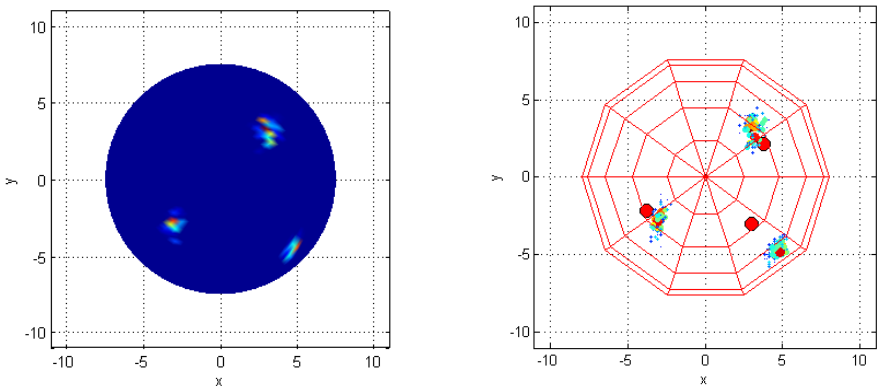

Figure 16: The reconstructed electric current intensity for three extended sources (red circles) at depth $S_d = 1\,cm$ when the shrinkage method was used. Here, $M = 2000$ and $N_t = 20$. Left: The electric intensity on the surface of the conducting sphere. Right: The electric intensity in the computational points. Just the points where the intensity is significant are shown.

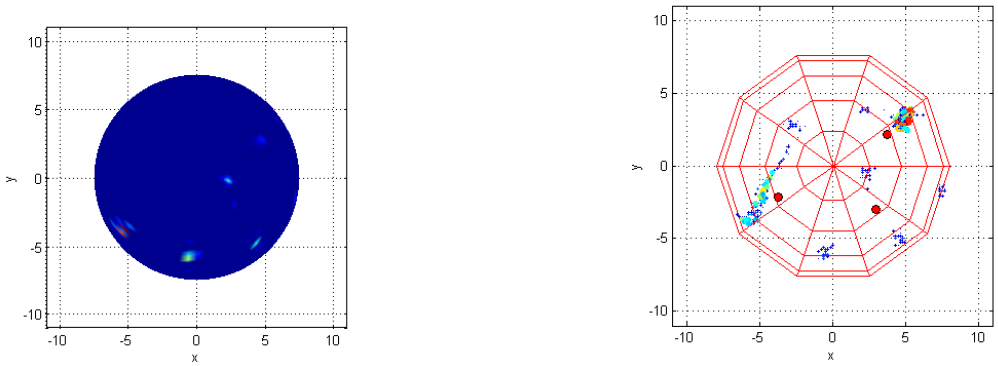

Figure 17: The reconstructed electric current intensity for three extended sources (red circles) at depth $S_d = 3\,cm$ when the shrinkage method was used. Here, $M = 2000$ and $N_t = 20$. Left: The electric intensity on the surface of the conducting sphere. Right: The electric intensity in the computational points. Just the points where the intensity is significant are shown.

5 Comments and conclusions

Neuroelectric source localization from MEG data is a challenging problem. For its solution many different algorithms, based on a variety of different frameworks and constraints, were proposed in the literature. In this paper, we introduce a new method which relies on the sparsity assumption. In fact, we assume that the electric current distribution inside the brain is spatially sparse so that just few localized elementary sources are sufficient to well reconstruct its image. These elementary sources have to be chosen randomly from a large dictionary, each source having the same probability of being selected at any time of the sampling process.

To show the performances of the proposed method several numerical tests were carried out. In the tests we used point-like delta functions as elementary sources and showed that few hundreds of these functions, uniformly distributed in the sphere, were sufficient to obtain a good localization of superficial electric sources, without the need to add any further constraints. In case of one deep source a shrinkage method based on ℓ_1-regularization is needed in order to improve the accuracy of the reconstruction, especially in case of noisy data. The tests showed also that the method is able to identify multiple sources, even if in this case the localization suffers from a shift toward the surface of the conducting sphere. This is more evident for deep weak sources. The shrinkage method does not improve the localization since it favors configurations where just one source, usually the strongest, is identified. Regularization methods suitable to deal with multiple deep sources are under study.

We notice that the random sampling method has a reduced computational load and takes just few seconds on a laptop. Moreover, the accuracy of the source localization can be improved just increasing the number of trials, which slightly increases the computing time but keeping the same memory storage. For these reasons the random sampling method can be effectively used in MEG source imaging and especially in real-time applications, such as brain-machine interfaces or neurofeedback rehabilitation after stroke or spinal cord injury ([12]). Numerical tests on real MEG data will be the subject of a forthcoming paper.

References

[1] V. Bruni, F. Pitolli, C. Pocci, A comparison of iterative thresholding algorithms for the MEG inverse problem, in press.

[2] I. Daubechies, M. Defrise, C. De Mol, An iterative thresholding algorithm for linear inverse problems with a sparsity constraint, Communications on pure and applied mathematics 57 (11) (2004) 1413–1457.

[3] C. Del Gratta, V. Pizzella, F. Tecchio, G. L. Romani, Magnetoencephalography - a noninvasive brain imaging method with 1 ms time resolution, Reports on Progress in Physics 64 (12) (2001) 1759.

[4] D. L. Donoho, Superresolution via sparsity constraints, SIAM Journal on Mathematical Analysis 23 (5) (1992) 1309–1331.

[5] H. W. Engl, M. Hanke, A. Neubauer, Regularization of inverse problems, vol. 375, Springer, 1996.

[6] M. Fornasier, F. Pitolli, Adaptive iterative thresholding algorithms for magnetoencephalography (MEG), Journal of Computational and Applied Mathematics 221 (2) (2008) 386–395.

[7] D. B. Geselowitz, On bioelectric potentials in an inhomogeneous volume conductor, Biophysical journal 7 (1) (1967) 1–11.

[8] D. B. Geselowitz, On the magnetic field generated outside an inhomogeneous volume conductor by internal current sources, Magnetics, IEEE Transactions on 6 (2) (1970) 346–347.

[9] M. Hämäläinen, R. Hari, R. J. Ilmoniemi, J. Knuutila, O. V. Lounasmaa, Magnetoencephalography – theory, instrumentation, and applications to noninvasive studies of the working human brain, Reviews of modern Physics 65 (2) (1993) 413.

[10] T. Hastie, R. Tibshirani, J. Friedman, T. Hastie, J. Friedman, R. Tibshirani, The Elements of Statistical Learning: Data Mining, Inference, and Prediction, Springer series in statistics Springer, Berlin, 2009.

[11] J. Kaipio, E. Somersalo, Statistical and computational inverse problems, vol. 160, Springer, 2005.

[12] G. Sudre, L. Parkkonen, E. Bock, S. Baillet, W. Wang, D. J. Weber, rt-MEG: a real-time software interface for magnetoencephalography, Computational intelligence and neuroscience 2011 (2011) 11.

[13] S. Supek, C. J. Aine, Magnetoencephalography. From Signals to Dynamic Cortical Networks, Springer, 2014.

[14] K. Wendel, O. Väisänen, J. Malmivuo, N. G. Gencer, B. Vanrumste, P. Durka, R. Magjarevic, S. Supek, M. L. Pascu, H. Fontenelle, et al., EEG/MEG source imaging: methods, challenges, and open issues, Computational intelligence and neuroscience 2009 (2009) 13.